Supplementary Information

Efficient Removal of Arsenate by a Versatile Magnetic Graphene Oxide Composites

Guodong Sheng[a,b], Yimin Li[a], Xin Yang[b], Xuemei Ren[b], Shitong Yang[b], Jun Hu[b], Xiangke Wang[b]*

[a]School of Chemistry and Chemical Engineering, Shaoxing University, Huancheng West Road 508, Shaoxing, Zhejiang 312000, P.R. China

[b]Key Laboratory of Novel Thin Film Solar Cells, Institute of Plasma Physics, Chinese Academy of Sciences, P.O. Box 1126, Hefei, 230031, P.R. China

List of Supporting Figures

List of Supporting Tables

Preparation of GO and MGO Composites. Graphene oxide (GO) was prepared from natural graphite by the modified Hummers method.[1-3] In brief, 1.0 g $NaNO_3$, 1.0 g graphite and 40 mL H_2SO_4 were mixed and stirred in a three neck flask in an acid bath, then 6 g $KMnO_4$ was added slowly. After that, the solution was transferred to a 35 ^oC water bath and stirred for ~1 h. Then 80 mL Milli-Q water was added and the solution was stirred for another 30 min at 90 ^oC. Then, 150 mL Milli-Q water and 6 mL H_2O_2 (30%) was added slowly, the color of solution turned from dark brown to yellow. The solution was filtered and rinsed with 100 mL Milli-Q water. The as-prepared GO was further treated with 3 mol/L HNO_3, which introduced hydrophilic functional groups (epoxy (C-O-C), hydroxyl (OH) and carboxyl (COOH)) at the surface of GO. The functionalized GO was further rinsed repeatedly with Milli-Q water to neutral pH values. The filter was vacuum dried and brown GO powder was thus obtained.

The MGO composites were synthesized by coprecipitation of $FeCl_3 \cdot 6H_2O$ and $FeCl_2 \cdot 4H_2O$ in the presence of GO. The mixed solution of $FeCl_3$ and $FeCl_2$ was added slowly to the GO solution, and ammonia solution was added quickly to precipitate Fe^{2+}/Fe^{3+} ions for the synthesis of magnetite (Fe_3O_4) particles. The temperature was raised to 85 ^oC, and a 30% ammonia solution was added to adjust the pH to 10. After being rapidly stirred for ~45 min, the solution was cooled to room temperature. The dark black colored solution was then filtered and rinsed with Milli-Q water/ethanol and dried in vacuum at 70 ^oC. The MGO composites were then prepared. The weight ratio of magnetite to GO was measured to be 4:1.[1]

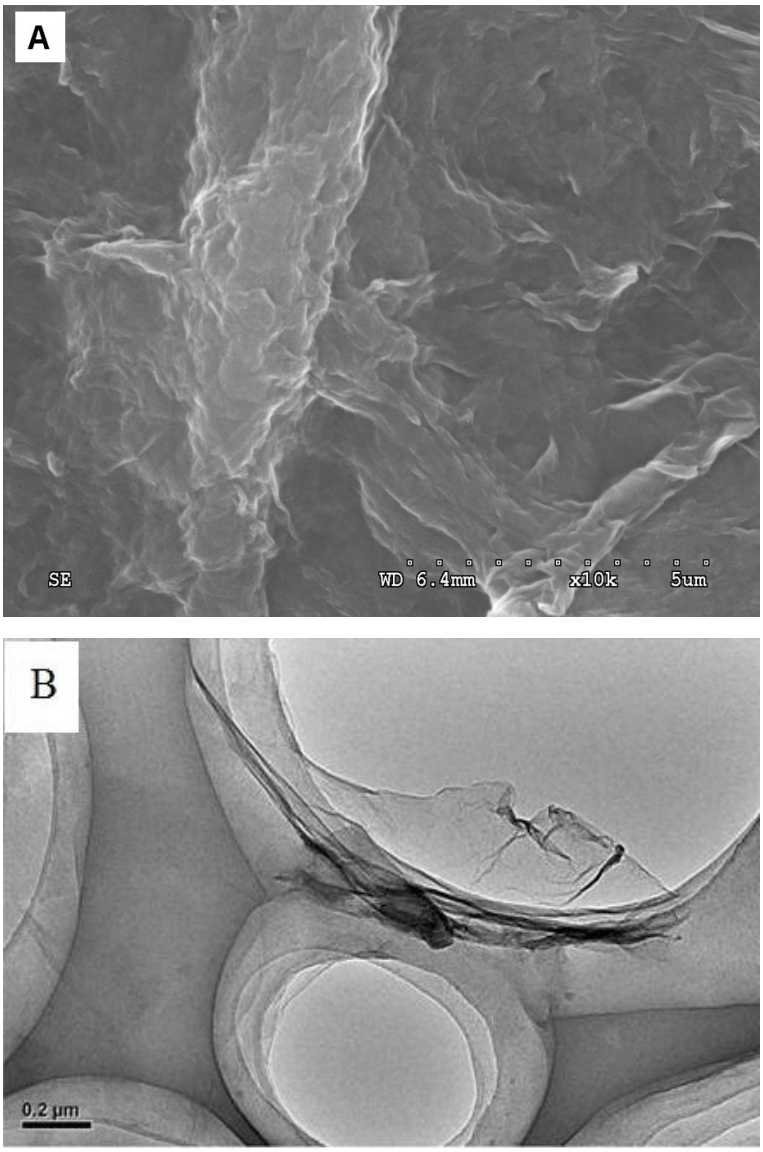

Fig. S1. (A) SEM and (B) TEM images of the GO sample.[4, 5]

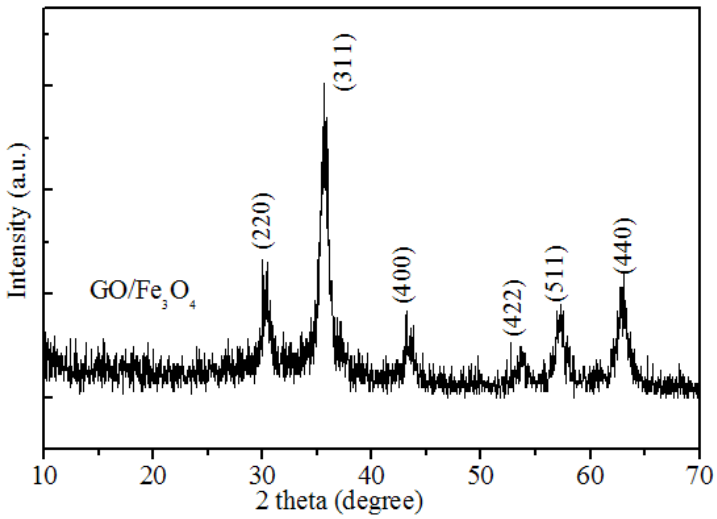

Fig. S2. XRD pattern of the MGO composites.[6]

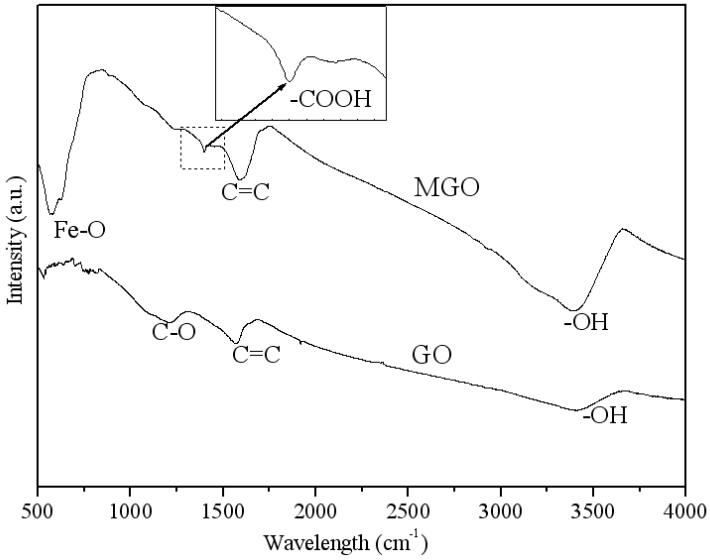

Fig. S3. FTIR spectra of the MGO composites[6] and GO samples.

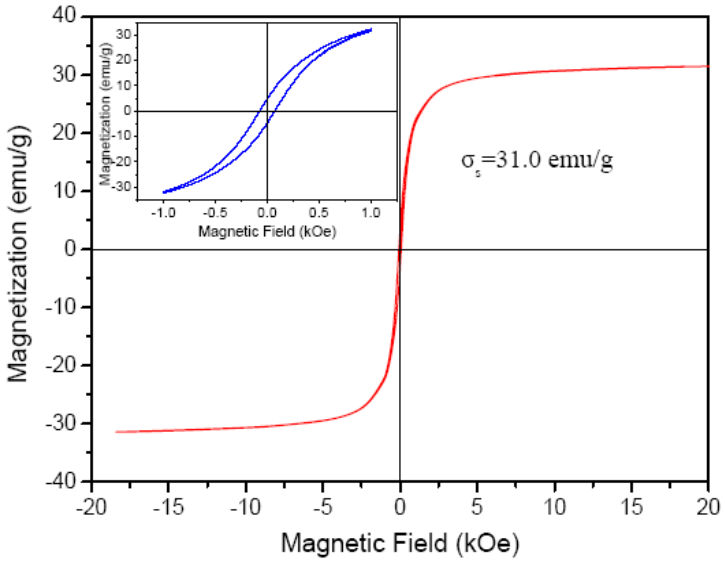

Fig. S4. Magnetization curve at room temperature of the MGO composites (Inset being separation of particles of MGO).[6]

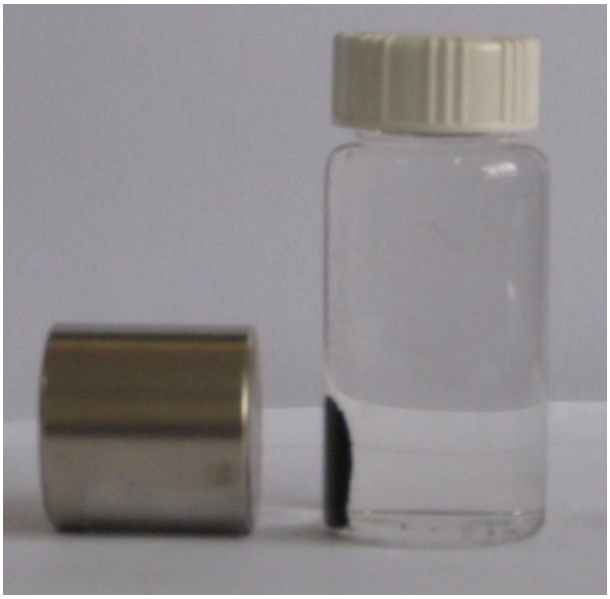

Fig. S5. Magnetic separation experiment of the MGO composites.

Table S1. Kinetic parameters of As(V) adsorption on MGO at pH=5.0 and 6.5.

pH	pseudo-second-order model			intra-particle diffusion model			
	q_e (mg/g)	K_2 (g/(mg·h))	R^2	$K_{p,1}$ (mg/(g·h))	R^2	$K_{p,2}$ (mg/(g·h))	R^2
5.0	61.4	0.02	0.997	27.1	0.991	0.53	0.911
6.5	29.5	0.05	0.998	10.4	0.988	0.52	0.915

Table S2. Langmuir and Freundlich fitting parameters of As(V) adsorption on MGO.

Conditions	Langmuir			Freundlich		
	q_{max} (mg/g)	B (L/g)	R^2	K_F ((mg^{1-n}L^n)/g)	n	R^2
T = 298 K, GO	80.1	0.06	0.989	8.6	0.53	0.967
T = 298 K, MGO	59.6	0.05	0.974	5.6	0.54	0.948
T = 298 K, Fe_3O_4	19.6	0.03	0.977	1.1	0.06	0.973
T = 318 K, MGO	63.2	0.07	0.972	8.9	0.47	0.932
T = 338 K, MGO	66.5	0.2	0.980	17.3	0.36	0.977

Table S3. Comparison of adsorption capacity of GO and MGO with other adsorbents for As(V).

Adsorbents	Experimental conditions	q_{max} (mg/g)	Ref.
Activated carbon	pH=8.0, T=303 K, m/V=0.2 g/L	43.7	7
Waste Fe(III)/Cr(III) hydroxide	pH=4.0, T=305 K, m/V=10 g/L	11.0	8
Iron coated pottery granules	pH=7.0	1.74	9
hydrous titanium dioxide	pH=4.0, T=293 K, m/V=0.1 g/L	33.4	10
Fe_3O_4-MWNTs based electrodes		53.2	11
Iron-containing mesoporous carbon	pH=7.8, T=298 K, m/V=3.0 g/L	5.5	12
Granular ferric hydroxide	pH=6.5, T=293 K, I=0.02 mol/L NaCl	3.1	13
perlite/α-MnO_2 nanocomposite	pH=7.0, T=293 K, m/V=2.0 g/L	7.1	14
perlite/γ-Fe_2O_3 nanocomposite	pH=7.0, T=293 K, m/V=2.0 g/L	4.6	14
Char-carbon	pH=7.5, T=298 K, m/V=5.0 g/L	30.5	15
Granular TiO_2	pH=7.0, T=293 K, m/V=1.0 g/L	41.4	16
Na-montmorillonite	pH=6.9, T=298 K, m/V=2.0 g/L	1.5	17
AC-modified montmorillonite	pH=6.9, T=298 K, m/V=2.0 g/L	3.4	17
PAC_{20}-modified montmorillonite	pH=6.9, T=298 K, m/V=2.0 g/L	3.6	17
Al_{13}-modified montmorillonite	pH=6.9, T=298 K, m/V=2.0 g/L	5.0	17
Clinoptilolite zeolite	pH=7.0, T=298 K, m/V=1 g/L	7.9	18
MnO_2-modified clinoptilolite zeolite	pH=7.0, T=298 K, m/V=1 g/L	33.8	18
Fe-exchanged natural zeolite	pH=6.0, T=298 K, m/V=0.2 g/L	50	19
Fe(II)-modified clinoptilolite	pH=7.0, T=296 K, m/V=0.2 g/L	40	20
Fe(III)-modified clinoptilolite	pH=7.0, T=298 K, m/V=0.25 g/L	44	21
Fe^{2+} oxide coated ethylenediamine functionalized MWCNT	pH=4.0, T=298 K, m/V=0.1 g/L	17.8	22
Fe^{3+} oxide coated ethylenediamine functionalized MWCNT	pH=4.0, T=298 K, m/V=0.1 g/L	10.4	22
Iron-containing granular activated carbon	pH=4.7, T=298 K, m/V=3.0 g/L	6.6	23
Iron-modified activated carbon	pH=8.0, T=293 K, m/V=0.1 g/L	43.6	24
GO	pH=6.5, T=298 K, m/V=0.4 g/L	80.1	This study
MGO	pH=6.5, T=298 K, m/V=0.4 g/L	59.6	This study

Table S4. Constants of linear fit of lnK_d vs. q_e (lnK_d=A+Bq_e) for As(V) adsorption on MGO.

T (K)	A	B	R
298	8.2	-0.0325	0.936
318	9.1	-0.0413	0.963
338	9.9	-0.0407	0.986

Table S5. Values of thermodynamic parameters for the adsorption of As(V) on MGO.

T (K)	$\Delta G°$ (kJ·mol^{-1})	$\Delta H°$ (kJ·mol^{-1})	$\Delta S°$ (J·mol^{-1}·K^{-1})
298	-20.4	35.2	
318	-23.9	35.4	189.9
338	-27.9	36.2	

Table S6. The initial pH and final pH in the adsorption system of As(V) onto MGO.

$pH_{initial}$	1.56	2.34	3.48	4.11	4.96	5.62	5.99	6.31	7.12	7.85	8.44	9.35	10.12	11.05	11.89
pH_{final}	1.60	2.41	3.55	4.22	5.02	5.68	6.06	6.37	6.76	7.33	7.95	8.46	9.78	10.12	10.55

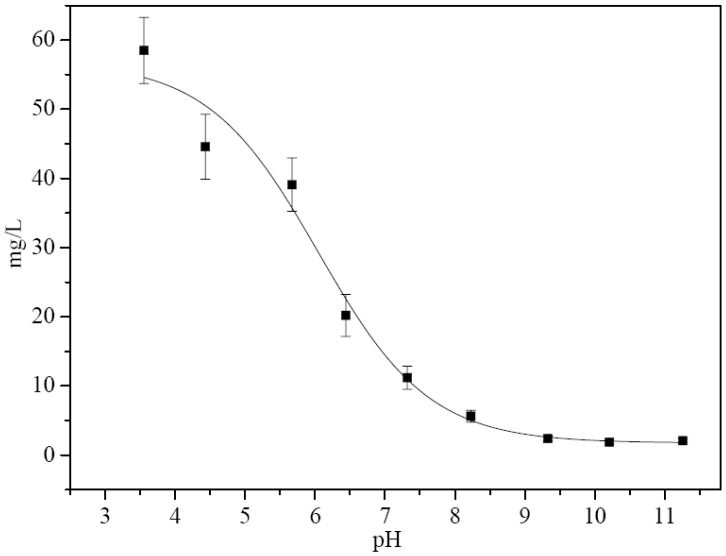

Fig. S6. The results of ferric ion dissolution experiment of the MGO composites as a function of solution pH, $[MGO]_0$=5 g/L.

Table S7. Adsorption of As(V) on MGO at pH 5.0 and 6.5 in the absence and presence of inorganic anions with various concentrations, T=298 K, $C_{[As(V)]}$=25 mg/L, m/V=0.4 g/L.

Anion	C_{anion} (mol/L)	pH=5.0		pH=6.5	
		As(V) adsorbed (mg/g)	IE (%)	As(V) adsorbed (mg/g)	IE (%)
No anion	0	55.6		27.6	
F^-	0.001	43.4	21.9	21.9	20.6
	0.01	36.8	33.8	18.3	33.5
	0.1	26.7	52.0	13.9	49.8
Cl^-	0.001	54.1	2.7	26.9	2.2
	0.01	53.8	3.8	26.7	3.3
	0.1	52.3	5.9	26.1	5.4
NO_3^-	0.001	54.7	1.6	27.3	1.1
	0.01	53.2	4.3	26.9	2.2
	0.1	51.4	7.5	26.4	4.3
SO_4^{2-}	0.001	50.5	9.1	25.8	6.5
	0.01	45.8	17.7	23.7	14.1
	0.1	40.4	27.4	20.4	25.9
HCO_3^-	0.001	49.1	11.8	25.2	8.7
	0.01	43.9	20.9	22.5	18.4
	0.1	30.2	29.5	20.7	24.9
HPO_4^{2-}	0.001	44.3	20.4	23.4	15.2
	0.01	34.4	38.1	17.1	37.9
	0.1	25.2	54.7	12.7	54.1

Table S8. Adsorption of As(V) on MGO at pH 5.0 and 6.5 in the absence and presence of organic anions with various concentrations, T=298 K, $C_{[As(V)]}$=25 mg/L, m/V=0.4 g/L.

Anion	C_{anion} (mg/L)	pH=5.0		pH=6.5	
		As(V) adsorbed (mg/g)	IE (%)	As(V) adsorbed (mg/g)	IE (%)
No anion	0	55.6		27.6	
OA	1	48.5	12.9	24.3	11.9
	10	42.2	24.1	21.0	23.8
	20	37.4	32.7	18.6	32.5
SA	1	49.6	10.7	25.2	8.7
	10	43.9	20.9	23.1	16.3
	20	35.6	35.9	19.8	28.1
MA	1	47.9	13.9	25.5	7.6
	10	42.8	23.1	22.2	19.5
	20	38.0	31.7	19.5	20.2
CA	1	48.5	12.9	24.6	10.8
	10	43.4	21.9	22.8	17.3
	20	37.7	32.2	20.1	27.1
HA	1	42.5	23.6	21.6	21.6
	10	35.9	35.4	18.0	34.6
	20	26.7	52.0	14.7	46.5
FA	1	41.9	24.7	22.5	18.4
	10	34.4	38.1	17.4	36.8
	20	26.9	51.5	13.9	49.8

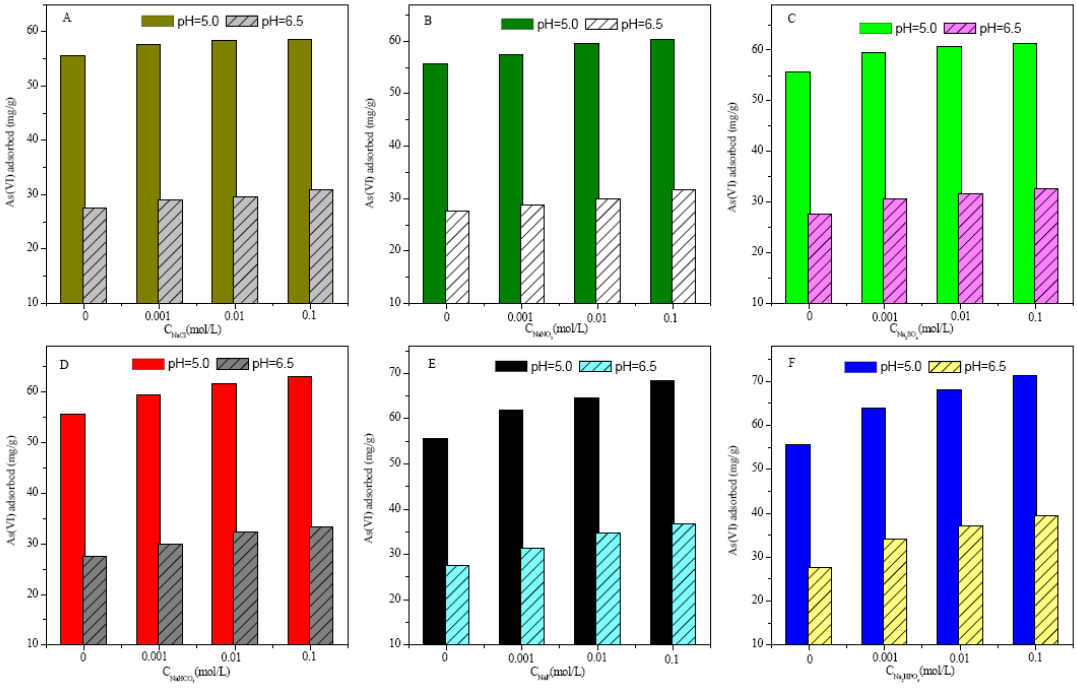

Fig. S7. Adsorption of As(V) on MGO at pH 5.0 and 6.5 in the absence and presence of coexisting cations with various concentrations, T=298 K, $C_{[As(V)]}$=25 mg/L, m/V=0.4 g/L, (A) K^+, (B) Na^+, (C) Ca^{2+}, (D) Mg^{2+}, (E) Al^{3+}, (F) Fe^{3+}.

Table S9. Adsorption of As(V) on MGO at pH 5.0 and 6.5 in the absence and presence of coexisting cations with various concentrations, T=298 K, $C_{[As(V)]}$=25 mg/L, m/V=0.4 g/L.

Cation	C_{cation} (mol/L)	pH=5.0		pH=6.5	
		As(V) adsorbed (mg/g)	EE (%)	As(V) adsorbed (mg/g)	EE (%)
No cation	0	55.6		27.6	
K^+	0.001	57.7	3.8	29.1	5.4
	0.01	58.3	4.8	29.7	7.6
	0.1	58.6	5.4	30.9	11.9
Na^+	0.001	57.4	3.2	28.8	4.3
	0.01	59.5	6.9	29.9	8.7
	0.1	60.4	8.6	31.8	15.2
Ca^{2+}	0.001	59.5	6.9	30.6	10.8
	0.01	60.7	9.1	31.8	15.2
	0.1	61.3	10.2	32.6	18.4
Mg^{2+}	0.001	59.5	6.9	29.9	8.7
	0.01	61.6	10.7	32.3	17.3
	0.1	63.1	13.4	33.2	20.6
Al^{3+}	0.001	61.9	11.3	31.5	14.1
	0.01	64.6	16.1	34.7	25.9
	0.1	68.4	23.1	36.8	33.5
Fe^{3+}	0.001	63.9	15.0	34.1	23.8
	0.01	68.1	22.5	37.1	34.6
	0.1	71.4	28.4	39.5	43.3

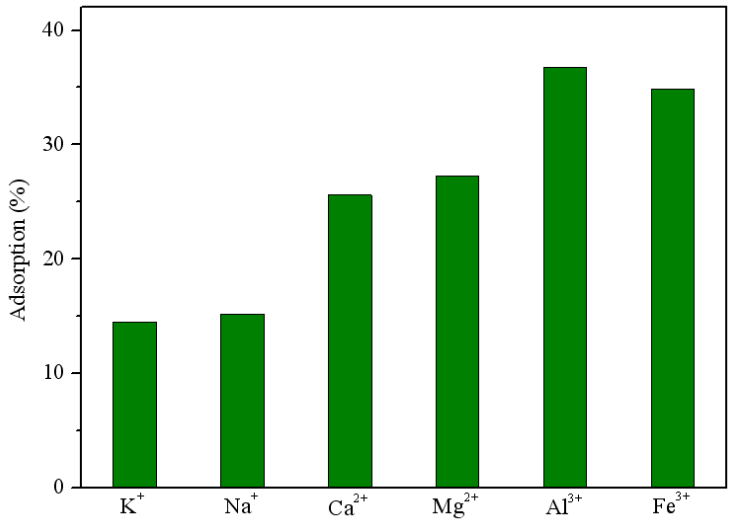

Fig. S8. Adsorption of cations (K^+, Na^+, Ca^{2+}, Mg^{2+}, Al^{3+}, Fe^{3+}) on MGO.

Impact of Adsorbent Content

The impact of MGO content on As(V) adsorption at pH=5.0 and 6.5 is shown in Figure S3. It can be found that the adsorption capacity decreases with MGO content increasing. When the MGO content increases from 0.1 to 0.8 g/L, the adsorption capacity decreases from 133.5 mg/L to 25.8 mg/L at pH=5.0, and from 70.5 mg/L to 21.7 mg/L at pH=6.5, respectively. This phenomena can be attributed to the following factors: (1) a higher amount of MGO effectively reduces the unsaturation of the available sites and correspondingly, the number of such sites per unit mass comes down, which results in less adsorption at higher MGO content; (2) when MGO content is low, As(V) can easily access to the adsorbing sites and thus results in high q_e values. With the rise in MGO content, the corresponding increase in adsorption per unit mass is less because of lower adsorption capacity utilization of the adsorbent, which may be ascribed to overcrowding of particles that may be termed as a kind of solid concentration effect; (3) higher MGO content creates particle aggregation, resulting in a decrease in the total surface area and an increase in diffusional path length which contributes to the decrease in adsorption capacity.[25] The adsorption percentage (%) of As(V) increases with increasing MGO content. This is reasonable because the higher MGO content can provide more adsorbing sites and thereby increases As(V) adsorption.[22] From Figure S4, it is clear that the concentration of As(V) remained in solution decreases with MGO content increasing. When the MGO content increases from 0.1 to 0.8 g/L, the concentration of As(V) remained in solution decreases from 11.7 mg/L to 4.4 mg/L at pH=5.0, and from 17.9 mg/L to 7.7 mg/L at

pH=6.5, respectively. This is certainly a capacity effect.[25] The distribution coefficient (K_d) does not change with MGO content increasing, which is consistent with the physicochemical properties of K_d, i.e., the K_d value is independent of solid content at low concentrations.[1]

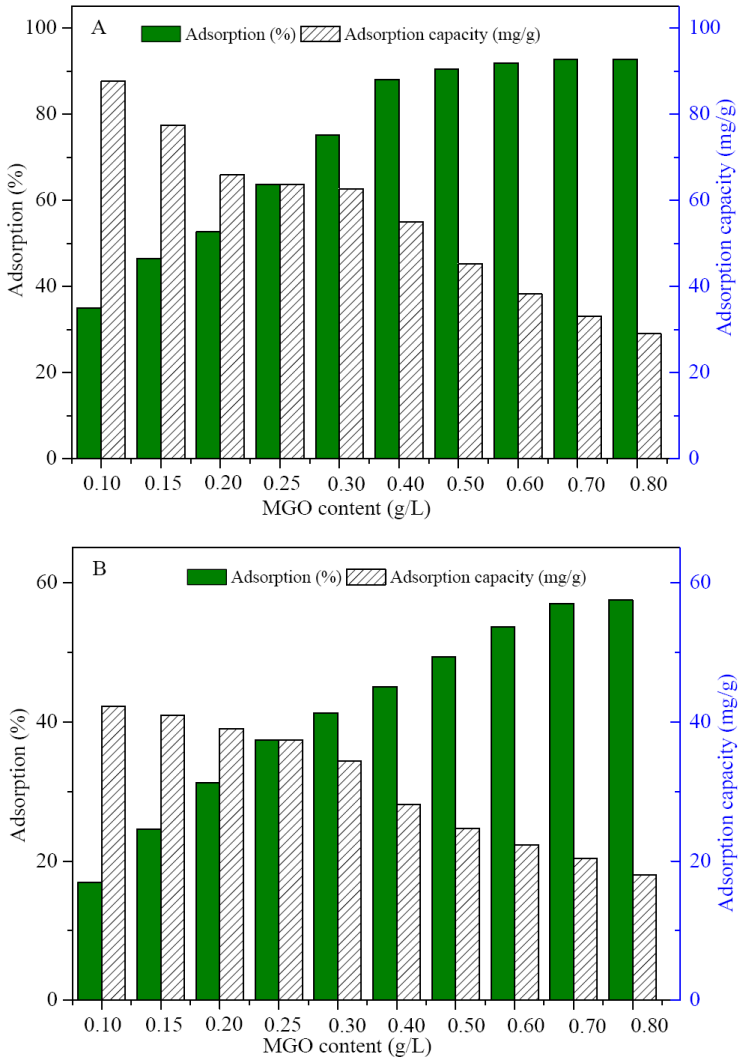

Fig. S9. Impact of adsorbent content on adsorption percentage and adsorption capacity of As(V) adsorption on MGO, $C_{[As(V)]}$=25 mg/L, T=298 K, (A) pH=5.0, (B) pH=6.5.

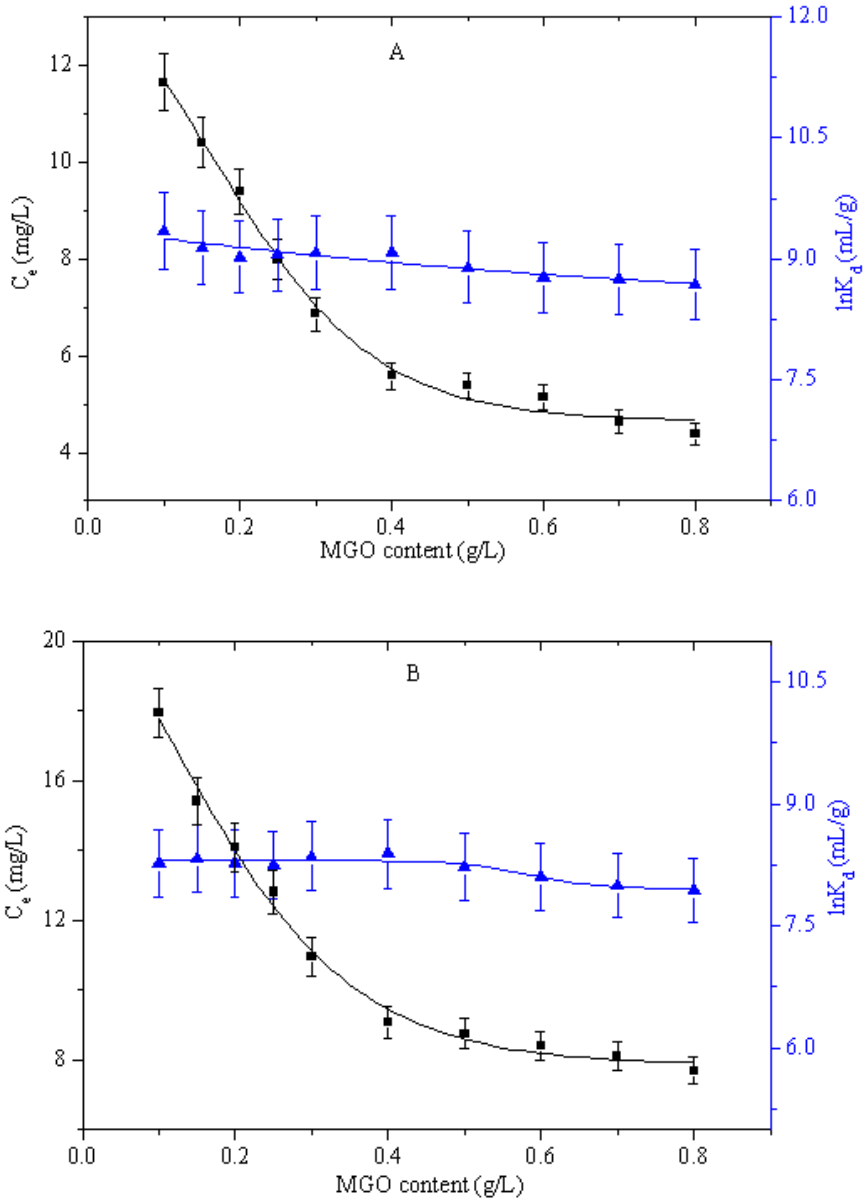

Fig. S10. Impact of adsorbent content on equilibrium concentration and distribution coefficient of As(V) adsorption on MGO, $C_{[As(V)]}$=25 mg/L, T=298 K, (A) pH=5.0, (B) pH=6.5.

REFERENCES

(1) Liu, M.; Chen, C.; Hu, J.; Wu, X.; Wang, X. Synthesis of magnetite/graphene oxide composite and application for cobalt(II) removal. *J. Phys. Chem. C* **2011**, *115*, 25234-25240.

(2) Hummers, W. S.; Offeman, R. E. Preparation of graphitic oxide. *J. Am. Chem. Soc*. **1958**, *80*, 1339-1341.

(3) Jahan, M.; Bao, Q. L.; Yang, J. X.; Loh, K. P. Structure-directing role of graphene in the synthesis of metal-organic framework nanowire. *J. Am. Chem. Soc*. **2010**, *132*, 14487-14495.

(4) Zhao, G.; Li, J.; Ren, X.; Chen, C.; Wang, X. Few-layered graphene oxide nanosheets as superior sorbents for heavy metal ion pollution management. *Environ. Sci. Technol*. **2011**, *45*, 10454-10462.

(5) Zhao, G.; Ren, X.; Gao, X.; Tan, X.; Li, J.; Chen, C.; Huang, Y.; Wang, X. Removal of Pb(II) ions from aqueous solutions on few-layered graphene oxide nanosheets. *Dalton Trans*. **2011**, *40*, 10945-40952.

(6) Yang, X.; Chen, C.; Li, J.; Zhao, G.; Ren, X.; Wang, X. Graphene oxide-iron oxide and reduced graphene oxide-iron oxide hybrid materials for the removal of organic and inorganic pollutants. *RSC Adv*. DOI: 10.1039/c2ra20885g.

(7) Liu, Z.; Zhang, F.; Sasai, R. Arsenate removal from water using Fe_3O_4-loaded activated carbon prepared from waste biomass. *Chem. Eng. J*. **2010**, *160*, 57-62.

(8) Namasivayam, C.; Senthilkumar, S. Removal of arsenic(V) from aqueous solution using industrial solid waste: adsorption rates and equilibrium studies. *Ind. Eng. Chem.*

Res. **1998**, *37*, 4816-4822.

(9) Dong, L.; Zinin, P. V.; Cowen, J. P.; Ming, L. C. Iron coated pottery granules for arsenic removal from drinking water. *J. Hazard. Mater*. **2009**, *168*, 626-632.

(10) Pirilä, M.; Martikainen, M.; Ainassaari, K.; Kuokkanen, T.; Keiski, R. L. Removal of aqueous As(III) and As(V) by hydrous titanium dioxide. *J. Colloid Interf. Sci*. **2011**, *353*, 257-262.

(11) Mishra, A. K.; Ramaprabhu, S. Magnetite decorated multiwalled carbon nanotubes based super capacitor for arsenic removal and desalination of sea water. *J. Phys. Chem. C* **2010**, *114*, 2583-2590.

(12) Gu, Z.; Deng, B. Use of iron-containing mesoporous carbon (IMC) for arsenic removal from drinking water. *Environ. Eng. Sci*. **2007**, *24*, 113-121.

(13) Banerjee, K.; Amy, G. L.; Prevost, M.; Nour, S.; Jekel, M.; Gallagher, P. M. Kinetic and thermodynamic aspects of adsorption of arsenic onto granular ferric hydroxide (GFH). *Water Res*. **2008**, *42*, 3371-3378.

(14) Thanh, D. N.; Singh, M.; Ulbrich, P.; Strnadova, N.; Štepánek, F. Perlite incorporating γ-Fe_2O_3 and α-MnO_2 nanomaterials: Preparation and evaluation of a new adsorbent for As(V) removal. *Sep. Purif. Technol*. **2011**, *82*, 93-101.

(15) Pattanayak, J.; Mondal, K.; Mathew, S.; Lalvani, S. B. A parametric evaluation of the removal of As(V) and As(III) by carbon-based adsorbents. *Carbon* **2000**, *38*, 589-596.

(16) Bang, S.; Patel, M.; Lippincott, L.; Meng, X. Removal of arsenic from groundwater by granular titanium dioxide adsorbent. *Chemosphere* **2005**, *60*,

389-397.

(17) Zhao, S.; Feng, C.; Huang, X.; Li, B.; Niu, J.; Shen, Z. Role of uniform pore structure and high positive charges in the arsenate adsorption performance of Al_{13}-modified montmorillonite. *J. Hazard. Mater*. **2012**, *203-204*, 317- 325.

(18) Camacho, L. M.; Parra, R. R.; Deng, S. Arsenic removal from groundwater by MnO_2-modified natural clinoptilolite zeolite: Effects of pH and initial feed concentration. *J. Hazard. Mater*. **2011**, *189*, 286-293.

(19) Li, Z.; Jean, J.; Jiang, W.; Chang, P.; Chen, C.; Li, L. Removal of arsenic from water using Fe-exchanged natural zeolite. *J. Hazard. Mater*. **2011**, *187*, 318-323.

(20) Payne, K. B.; Abdel-Fattah, T. M. Adsorption of arsenate and arsenite by iron treated activated carbon and zeolites: Effects of pH, temperature, and ionic strength. *J. Environ. Sci. Health* **2005**, *40*, 723-749.

(21) Habuda-Staniæ, M.; Kalajdziæ, B.; Kuleš, M.; Veliæ, N. Arsenite and arsenate sorption by hydrous ferric oxide/polymeric material. *Desalination* **2008**, *229*, 1-9.

(22) Velivckovic, Z.; Vukovic, G. D.; Marinkovic, A. D.; Moldovan, M. S.; Peric-Grujic, A. A.; Uskokovic, P. S.; Ristic, M. D. Adsorption of arsenate on iron(III) oxide coated ethylenediamine functionalized multiwall carbon nanotubes. *Chem. Eng. J*. **2012**, *181*, 174-181.

(23) Gu, Z.; Fang, J.; Deng, B. Preparation and evaluation of GAC-based iron-containing adsorbents for arsenic removal. *Environ. Sci. Technol*. **2005**, *39*, 3833-3843.

(24) Chen, W.; Parette, R.; Zou, J.; Cannon, F. S.; Dempsey, B. A. Arsenic removal by

iron modified activated carbon. *Water Res*. **2007**, *41*, 1851-1858.

(25) Sheng, G.; Hu, J.; Jin, H.; Yang, S.; Ren, X.; Li, J.; Chen, Y.; Wang, X. Effect of humic acid, fulvic acid, pH, ionic strength and temperature on ^{63}Ni(II) sorption to MnO_2. *Radiochimica Acta* **2010**, *98*, 291-299.